constants were calculated.[38] Analogous equilibria are believed to exist in the molten-salt systems studied here, where $AlCl_4^-$, $Al_2Cl_7^-$ and possibly $Al_3Cl_{10}^-$ assist in the solution process; we consider, however, the spectral precision achievable in the present difficult system to be inadequate for equilibrium quantification. The breadth of the bands G-I in Figure 2 must reflect the presence of multiple species of very different donor strengths if only two species are present.

Concluding Remarks

(1) The relative efficacies of the spectroscopic probes Tl^+, Pb^{2+}, and Bi^{3+} for detecting changes in the thermodynamic state of these chloroaluminate acid–base systems seem consistent with experience with conventional protonic acid–base indicators; viz., the best indicator for a process is the one with a basicity midway between the extremes. Here the extremes of basicity are determined by the polarization resulting from monovalent cations at one extreme and trivalent Al^{3+} at the other. Thus Pb^{2+}, with an intermediate field strength is best, while Tl^+ is unconscious of the equivalence point. To probe less pronounced basicity changes in a system such as $ZnCl_2 + AlCl_3$ (in which Co^{2+} coordination changes have been induced by composition variations[40]) it is probable that Pb^{2+} would be insensitive but Bi^{3+} would serve well as a probe.

(2) The magnitude of the electronic energy change from acidic to basic conditions is of interest. Changing the chloride ions with which the probes interact from Al^{3+}-polarized to Li/K-polarized in the LiCl–KCl eutectic results in changes in the photon energy needed to promote the $^3P_1 \leftarrow {}^1S_0$ transition amounting to 0.333, 0.313, and 0.562 eV for the Bi^{3+}, Pb^{2+}, and Tl^+ ions, respectively. Since it is the same change in electronic polarization state that provides the free-energy driving force for the acid–base process, e.g. in $AlCl_3 + KCl$, it is perhaps not surprising to observe that the free-energy change determined by electrochemical or other means at the equivalence point is of the same order $\Delta G = 2.303(RT/F)[\Delta(pCl)] = 0.57$ eV for the case $AlCl_3 + KCl$. For the case of Bi^{3+} in $AlCl_3 + KCl$, see Figure 4, the change in excitation energy across the 50% equivalence point, 4720 cm^{-1}, is in fact 0.59 eV.

Acknowledgment. This work was supported by the National Science Foundation under Solid State Chemistry Grant Nos. DMR 77-04318A1 and 8007052A2. We are grateful to Dr. M. D. Ingram for his careful review of this work and the many stimulating discussions.

(40) C. A. Angell and D. M. Gruen, *J. Inorg. Nucl. Chem.*, **29**, 2243 (1967).

Contribution from the Inorganic Chemistry Laboratory, Oxford University, Oxford OX1 3QR, England

Phonons in Mixed-Valency and Mixed-Metal Salts $A_2M_{0.5}Sb_{0.5}Cl_6$ (A = Rb, Cs; M = Sb, Bi, Tl): An Inelastic Neutron Scattering Study

KOSMAS PRASSIDES and PETER DAY*

Received October 16, 1984

Incoherent inelastic neutron scattering has been used to measure the phonon density of states (dos) of the mixed-valency and mixed-metal salts $A_2M_{0.5}Sb_{0.5}Cl_6$ (A = Rb, Cs; M = Sb, Bi, Tl) from 0 to 360 cm^{-1}, i.e. up to and including the intramolecular stretching modes. Similar measurements were also made on the cubic model compound Cs_2SnCl_6 and mixed-valency $Rb_{2.67}SbCl_6$. To assign the peaks in the frequency-dependent dos, a rigid-ion model was used to fit zone-center phonon frequencies previously available from infrared and Raman spectroscopy to a set of force constants and ionic charges. The latter were used to calculate phonon dispersion relations and a model dos for each compound. Above 110 cm^{-1} the measured dos are dominated by zone-center intramolecule modes of MCl_6^{3-} and $SbCl_6^-$ while in the region of the lattice modes the dos of all the salts are very similar. Consistent with the strong electron localization in the ground state, there are no features in the phonon dos of Cs_2SbCl_6 specifically assignable to mixed valency. The relevance of the phonon dos data to the quantitative interpretation of the intervalence absorption band shape is briefly discussed.

Introduction

The hexahalogenoantimonate(III,V) salts have long been recognized as prototypes of Robin–Day[1] class II mixed-valency behavior. Their structural simplicity makes them ideal starting models for an understanding of the dynamics of intervalence electron transfer in weak interaction mixed-valency systems. A detailed study of the temperature dependence of the shape[2] of the Franck–Condon optical charge-transfer profile in $(CH_3NH_3)_2Sb^{III}_{x/2}Sb^{V}_{x/2}Sn^{IV}_{1-x}Cl_6$ and its low-energy tail[3] in $Rb_{2.67}SbCl_6$ indicates that both lattice and intramolecular vibrational modes are involved in varying the lattice potential energy around the two Sb sites, and thus coupling to the electron transfer from Sb(III) to Sb(V). Consistent with this analysis are the resonance Raman results on Cs_2SbCl_6,[4] indicating the resonance enhancement of a lattice mode, and on $Cs_2Sb_xSn_{1-x}Cl_6$,[5] whence some $Sn^{IV}Cl_6^{2-}$ vibrations are similarly resonance enhanced. Furthermore, the gain in elastic energy associated with the strong electron–phonon coupling in these systems is responsible for overcoming the unfavorable repulsion of the two electrons occupying the same orbital.

Information about the phonon modes in mixed-valency compounds has come so far from infrared and Raman spectroscopy,[4,6,7] but these are confined by the selection rules to modes close to the Brillouin zone center, whereas information about the complete phonon density of states (dos) across the Brillouin zone is required in order to estimate the lattice elastic and Coulomb energy. The most suitable experimental method for such a study is inelastic neutron scattering (INS). Unfortunately the hexahalogenoantimonates(III,V) cannot be grown into large single crystals so INS experiments must be restricted to incoherent scattering (IINS). Given that hydrogen has an incoherent cross section ca. 20 times larger than any other element, IINS has mostly been used in studies of hydrogenous materials.[8] However, high-flux reactors and high-resolution spectrometers have recently made it possible to enlarge the range of possible experiments on weak or moderate incoherent neutron scatterers.

We have undertaken a detailed study of the phonon spectra of the mixed-valency $Cs_2Sb^{III}_{0.5}Sb^{V}_{0.5}Cl_6$ and mixed-metal $Cs_2Bi^{III}_{0.5}Sb^{V}_{0.5}Cl_6$, $Cs_2Tl^{III}_{0.5}Sb^{V}_{0.5}Cl_6$, $Rb_2Tl^{III}_{0.5}Sb^{V}_{0.5}Cl_6$ salts by IINS. Due to superlattice ordering,[9] the primitive unit cell in these

(1) Robin, M. B.; Day, P. *Adv. Inorg. Chem. Radiochem.* **1967**, *10*, 247.
(2) Prassides, K.; Day, P. *J. Chem. Soc., Faraday Trans. 2* **1984**, *80*, 85.
(3) Prassides, K.; Day, P. *J. Chem. Soc., Faraday Trans. 2*, in press.
(4) Clark, R. J. .; Trumble, W. R. *J. Chem. Soc., Dalton Trans. 1976*, 1145.
(5) Clark, H. W.; Swanson, B. J. *J. Am. Chem. Soc.* **1979**, *101*, 1604.
(6) Barrowcliffe, T.; Beattie, I. R.; Day, P.; Livingstone, K. *J. Chem. Soc. A* **1967**, 1810.
(7) Clark, H. W.; Swanson, B. I. *J. Am. Chem. Soc.* **1981**, *103*, 2928.
(8) Howard, J.; Waddington, T. C. *Adv. Infrared Raman Spectrosc.* **1980**, *7*, 86.

0020-1669/85/1324-3035$01.50/0

Table I. Observed Frequencies of Phonon Spectra of Cs_2SnCl_6 (cm^{-1})

peak	bfd/12 K	tof/80 K	tof/295 K	assgnt
K		28		L^{3-} (TA)
I		32	33	X^{5-} (TA)
G		50	46	LCs^{+} (Γ^{5+}), L^{2-} (LA)
F		67	65	L^{2+} (Rot), X^{5+} (Rot)
E	74	80	70	TO (Γ^{4-})
D	124	125	122	X^{5-} ($T\nu_6$), X^{3-} ($L\nu_6$)
C	176	170	166	Γ^{5+}, Γ^{4-} (ν_4)
B	242	245	233	Γ^{2+}, X^{1+} (ν_2)
A	323		303	Γ^{1+}, Γ^{4-} (ν_1)

materials is quite large. Thus we start by investigating the related cubic single-valence compound $Cs_2Sn^{IV}Cl_6$.

Experimental Section

All the compounds were prepared by standard methods[10,11] from concentrated HCl solutions of the constituent ions.

Initial IINS spectra of Cs_2SnCl_6 and Cs_2SbCl_6 were obtained on the beryllium-filter detector (bfd) spectrometer[12] at the DIDO reactor, AERE Harwell, England. The bfd spectrometer uses neutron energy loss, and spectra were recorded at 12 K to minimize multiphonon contributions to the background. The samples were contained in sachets of 0.002-in. aluminum foil. A thin Cd piece was attached to the bottom of the sample to ensure good alignment. Incident neutron energies between 12 and 50 meV were scanned in 1 meV steps by using the (111) plane of the aluminum monochromator. The data were normalized to constant monitor counts and corrected for instrumental scattering by subtracting an empty sample sachet scan. The true transition values were obtained by applying appropriate correction factors.[13]

Time-of-flight (tof) IINS spectra of Cs_2SnCl_6 (80 K, 295 K), Cs_2SbCl_6 (80 K, 295 K), $Cs_2Bi_{0.5}Sb_{0.5}Cl_6$ (80 K), $Cs_2Tl_{0.5}Sb_{0.5}Cl_6$ (295 K), $Rb_2Tl_{0.5}Sb_{0.5}Cl_6$ (295 K), and $Rb_{2.67}SbCl_6$ (80 K) were recorded by the time-focusing IN6 spectrometer[14] at the Institut Laue-Langevin, Grenoble, France. IN6 is a neutron-energy-gain spectrometer, and to obtain sufficient thermal population of phonon states, spectra were originally recorded at 295 K. This results in an appreciable multiphonon background. Spectra were later recorded at 80 K, and even though the population of low-lying phonon states has increased, a marked increase in resolution at low energy transfer results; only at energy transfers greater than ca. 200 cm^{-1} is the resolution worse than at 295 K. Neutron wavelengths of 4.1 and 5.1 Å were used for the 295 and 80 K runs, respectively. Corrections were made for instrumental background by running an empty sample can. A vanadium run was used as calibrant, allowing determination of the relative efficiencies of the counters. In the recording of the tof spectra, the detectors were grouped in 13 sets. In general, the observed transitions show very little dispersion (scattering angles between 13 and 110°), especially the intramolecular vibrations. In order to improve data statistics, the spectra from all 13 angles of detection were summed, with loss of momentum transfer resolution. The tof spectra were analyzed by using standard computer programs[15] and are presented as phonon frequency distribution function $\sum P(\alpha,\beta)$ vs. energy transfer, where

$$P(\alpha,\beta) = 2\beta[\sinh(\beta/2)]S(\alpha,\beta)/\alpha \qquad (1)$$

and $\alpha = \hbar Q^2/2mkT$, $\beta = \hbar\omega/kT$, Q is the momentum transfer, $S(\alpha,\beta)$ is the incoherent scattering law, m is the mass of the scattering atom, k is Boltzmann's constant, $\hbar$ is Planck's constant, ω is the frequency of the transition, and T is the temperature.

Results

Figure 1 presents the experimental frequency distribution functions $\sum P(\alpha,\beta)$ vs. energy transfer for the salts studied at an average scattering angle of 59°. $P(\alpha,\beta)$[8] is related to the phonon density of states $g(\omega)$ by weighting with the incoherent scattering cross sections, σ_{incoh} of the individual elements,[16] the amplitudes

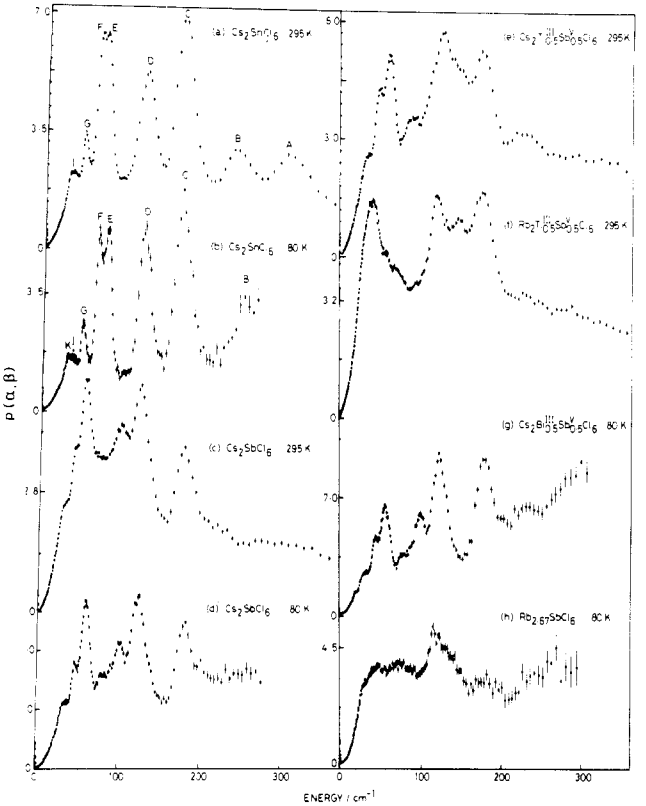

Figure 1. Phonon frequency distribution functions $P(\alpha,\beta)$ of (a) Cs_2SnCl_6 at 295 K, (b) Cs_2SnCl_6 at 80 K, (c) Cs_2SbCl_6 at 295 K, (d) Cs_2SbCl_6 at 80 K, (e) $Cs_2Tl_{0.5}Sb_{0.5}Cl_6$ at 295 K, (f) $Rb_2Tl_{0.5}Sb_{0.5}Cl_6$ at 295 K (g) $Cs_2Bi_{0.5}Sb_{0.5}Cl_6$ at 80 K, and (h) $Rb_{2.67}SbCl_6$ at 80 K.

of vibration, $|u_l^{\alpha}|$, and the Debye–Waller factor, $\exp[2W_l(\omega_\alpha)]$. Despite the difficulties associated with low-scattering and large absorption cross sections in a non-hydrogenous sample, IN6 permits measurements of excellent IINS spectra by using moderate quantities of powder, ca. 5 g, (cf. 25 g used in filter spectroscopy), and counting for only 10 h.

The peak frequencies are summarized together with the bfd results in Table I.

Discussion

To assign the phonon spectra of Cs_2SnCl_6 and of the mixed-valency and mixed-metal compounds, we utilize a rigid-ion lattice dynamics model to calculate model phonon dos. Some initial knowledge of the force constant parameters of the bonds between the atoms in the primitive unit cell is required, so we first consider the available optical data, which are fitted to the rigid-ion model to estimate values for the force constants. This information is inserted in the dynamical matrix, which then can be diagonalized at points with wave vector $\mathbf{k}$ within the first Brillouin zone to give the dispersion relations $\omega(\mathbf{k})$ vs. $\mathbf{k}$. Integration over the Brillouin zone then results in a model phonon dos.

Rigid-Ion Model. Within a rigid-ion-model framework, the distortions of the individual ions during vibrations are neglected. Under this assumption, the potential energy Φ consists of a short-range part arising from the overlap of the electron distributions of neighboring ions only and a long-range Coulomb part.

In the O'Leary and Wheeler[17] (OLW) lattice dynamical model, the short range part of the potential is assumed to be axially symmetric and to involve only central interactions along single bonds, i.e.

$$\Phi^{SR}\left(\begin{smallmatrix}0 & l\\ \kappa & \kappa'\end{smallmatrix}\right) = \Phi^{SR}(\mathbf{R}) \qquad (2)$$

where $\mathbf{R} = |\mathbf{X}(^{l}_{\kappa'}) - \mathbf{X}(^{0}_{\kappa})|$ with $\mathbf{X}(^{l}_{\kappa})$ being the position vector of

(9) Prassides, K.; Day, P.; Cheetham, A. K. *J. Am. Chem. Soc.* **1983**, *105*, 3366. Prassides, K.; Day, P.; Cheetham, A. K. *Inorg. Chem.* **1985**, *24*, 545.
(10) Day, P. *Inorg. Chem.* **1963**, *2*, 452.
(11) Atkinson, L.; Day, P. *J. Chem. Soc. A* **1968**, 2423.
(12) Harris, D. H. C.; Hill, R. I. Harwell Report HL82/3135, 1982.
(13) Gamlen, P. H.; Hall, N. F.; Taylor, A. D. Harwell Report PRL74/693, 1974.
(14) Dianoux, J. Institute Laue-Langevin Report 79D117T, 1979.
(15) Dianoux, J.; Ghosh, R. E.; Hepvet, H.; Lechner, R. E. Institut Laue-Langevin Report 75D16T, 1979.
(16) Bacon, G. E. "Neutron Diffraction"; Oxford University Press: London, 1975.
(17) O'Leary, G. P.; Wheeler, R. G. *Phys. Rev. B: Solid State* **1970**, *1*, 4409.

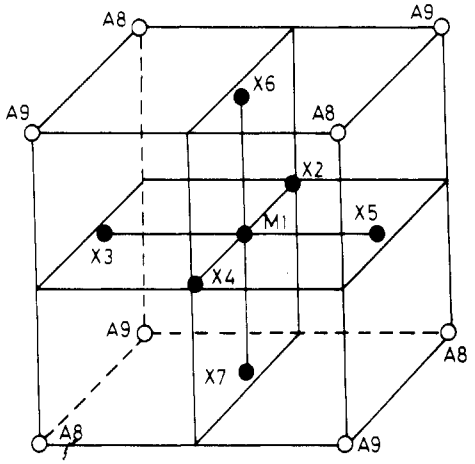

Figure 2. Primitive unit cell of face-centered-cubic A_2MX_6, showing the numbering scheme used in the model.[17]

the κth atom in the lth unit cell. The second derivative of the short-range potential energy Φ^{SR} with respect to R_α, the distance between sites κ and κ' along the αth axis is

$$\frac{\partial^2\Phi^{SR}(\mathbf{R})}{\partial R_\alpha \partial R_\beta} = \frac{1}{R}\Phi'_{SR}(\mathbf{R})\left[\delta_{\alpha\beta} - \frac{R_\alpha R_\beta}{R^2}\right] + \frac{R_\alpha R_B}{R^2}\Phi''_{SR}(\mathbf{R}) \equiv \Phi_\perp\left[\delta_{\alpha\beta} - \frac{R_\alpha R_B}{R^2}\right] + \Phi_\parallel \frac{R_\alpha R_\beta}{R^2} \quad (3)$$

Hence for each pair of interacting atoms, the corresponding short-range part of the dynamical matrix element is given in terms of the first and second derivatives of the potential, referred to as the perpendicular ($\Phi_\perp$) and parallel ($\Phi_\parallel$) force constants, respectively. The Coulomb contribution to the dynamical matrix can be calculated by Ewald's method.[18]

Cs_2SnCl_6 Phonon Spectra. The structure of Cs_2SnCl_6 can be viewed simply as the CaF_2 structure, wherein the Ca^{2+} ions are replaced by the rigid-body octahedra of $SnCl_6^{2-}$ and the F^- ions by the Cs^+ ions, though with rotational degrees of freedom of the solid octahedron $SnCl_6^{2-}$. The primitive unit cell of the antifluorite structure is shown in Figure 2. The atoms are numbered for later use in the model. The first Brillouin zone of the antifluorite structure is drawn in Figure 3. The number of molecular units in the primitive unit cell is 1 and the number of atoms 9, thus resulting in 27 normal modes of vibration for each wave vector **k**.

The original OLW model as applied to K_2ReCl_6 employed 14 parameters.[17] The number of parameters is directly related to the number of atom pairs assumed to interact via short-range forces. Each pair of interacting atoms provide one perpendicular and one parallel force constant (eq 3). Symmetry-related pairs of atoms interact with the same force constants, thus simplifying the problem. However, to base our model on optical spectroscopy, which is limited to modes at the zone center, we must reduce correspondingly the number of pairs of atoms that are taken to interact via short-range forces.

Of the zone-center vibrational modes, only three are infrared active: the stretching Sn–Cl Γ^{4-} (ν_3) internal mode, the bending Cl–Sn–Cl Γ^{4-} (ν_4) internal mode, and the Γ^{4-} optical mode. All three have been observed by infrared spectroscopy[7,19,20] (for the optical mode, the observed value refers to the transverse optical (TO) branch). Four more zone-center modes are Raman active: the totally symmetric Sn–Cl internal mode Γ^{1+} (ν_1), the stretching Sn–Cl Γ^{3+} (ν_2) internal mode, the bending Cl–Sn–Cl Γ^{5+} (ν_5) internal mode, and the Γ^{5+} lattice mode involving Cs^+ motion. All four modes have been observed by Raman spectroscopy.[19,20]

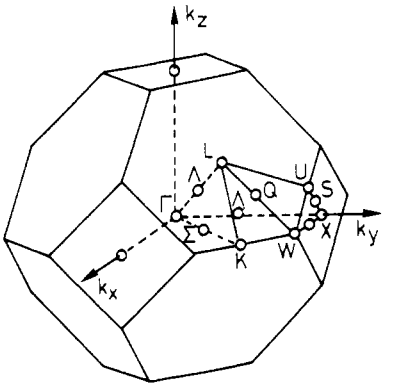

Figure 3. Face-centered-cubic Brillouin zone appropriate for Cs_2SnCl_6.

Two more modes are silent, the bending Cl–Sn–Cl Γ^{5-} (ν_6) internal mode and the rotary Γ^{4+} external mode. Thus optical spectroscopy yields seven frequencies.

To enumerate the independent parameters needed to describe the dynamical matrix in Cs_2SnCl_6, note that in the long-range part the effective charges of the six chlorine ions are equal by symmetry, as also are the two cesium charges. Further, electrical neutrality requires $2q_{Cs} + q_{Sn} + 6q_{Cl} = 0$. Hence there are only two independent parameters, the charges on Sn and Cl. Considering the short-range part of the dynamical matrix, we can restrict ourselves to the interactions within one octahedron in the primitive unit cell. Because of the high symmetry, there are only three independent bonds: between Sn and Cl (e.g. Sn(1)–Cl(2)), between nearest-neighbor Cl (e.g. Cl(2)–Cl(3)), and between axially symmetric Cl (e.g. Cl(2)–Cl(4)). Further, we include a Cs–Cl interaction (e.g. Cl(2)–Cs(8), all other Cs–Cl being equivalent by symmetry) and a Cs–Cs nearest-neighbor interaction, e.g. Cs(8)–Cs(9) ($^1/_2$, 0, $^1/_2$). Thus there are five independent pairs of atoms within each primitive unit cell, giving ten more independent parameters. Equilibrium conditions for the ionic lattice provide further constraints that limit the number of independent parameters. Thus, Boyer and Hardy[21] have considered explicitly the static equilibrium conditions for rigid-ion crystals; i.e., the static lattice must be in equilibrium, both with respect to any macroscopic strain and also with respect to relative motion of the constituent sublattices. In the antifluorite crystals, these conditions express two constraints on the perpendicular force constants, reducing the number of independent parameters to ten.

Since there are only seven observed values for the frequencies of the normal modes at the Γ point, no more bonding interactions can be included. Thus we exclude interactions between the Cl atoms on neighboring octahedra, though some are separated by distances comparable to those within a single octahedron and they are important in determining the rotary-mode eigenvalue correctly. Further, the perpendicular force constants of the bonds Cs(8)–Cs(9), Cl(2)–Cl(4), and Cs(8)–Cl(2) are set equal to zero and are not refined in the subsequent fitting procedure.

The computer program of Sutton[22,23] to calculate dispersion curves for any crystal structure within a rigid-ion model were run on the CRAY 1S computer at the University of London. The final values of the parameters of the least-squares fit are listed in Table II, with the observed and calculated values of the frequencies.

After insertion of the values of the force constants and charges, the dispersion relations for Cs_2SnCl_6 are calculated by repeated diagonalization of the dynamical matrix

$$|D_{ij}(\mathbf{k}) - \omega^2(\mathbf{k})\,\delta_{ij}| = 0 \quad i, j = 1\text{–}27 \quad (4)$$

The results along some high-symmetry lines of the Brillouin zone are shown in Figure 4. When the symmetry-adapted coordinates[23]

(18) Ewald, P. P. *Ann. Phys.* **1921**, *64*, 253.
(19) Adams, D. M.; Morris, D. M. *J. Chem. Soc. A* **1967**, 1666.
(20) Debeau, M.; Poulet, H. *Spectrochim. Acta, Part A* **1969**, *25*, 1553.
(21) Boyer, L. L.; Hardy, J. R. *Phys. Rev. B: Solid State* **1973**, *7*, 2886.
(22) Sutton, M. Ph.D. Thesis, University of Toronto, 1981.
(23) Sutton, M.; Armstrong, R. L.; Powell, B. M.; Buyers, W. J. L. *Phys. Rev. B: Condens. Matter* **1983**, *27*, 380.

Table II. Lattice Dynamics Parameters for Cs_2SnCl_6

atom	charges/e	
	model I	model II
Sn	1.20	0.89
Cl	−0.40	−0.30
Cs	0.60	0.46

	force constant/N m^{-1}			
	model I		model II	
	parallel	perpendicular	parallel	perpendicular
Cs(8)–Cs(9)	−0.19	0	−0.16	0
Cl(2)–Cl(4)	2.24	0	1.38	0
Cs(8)–Cl(2)	6.08	0	6.49	0
Cl(2)–Cl(3)	17.89	−4.04	20.15	−3.25
Sn(1)–Cl(2)	124.35	11.12	116.75	10.23

	freq/cm^{-1}		
	obsd	model I	model II
Q_3	313	313	313
Q_1	310	310	310
Q_2	243	243	243
Q_4	172	172	170
Q_5	168	168	172
$TQ_6(X^{5-})$	122[a]	109	119
TO	69	69	71
LCs^+	53	53	53

[a] Not used in model I.

are compared with the calculated eigenvectors from the model,[24] there is little evidence of mode mixing at the Γ point. However, there is considerable mode mixing away from Γ; e.g., the longitudinal acoustic and the longitudinal optical (LO) modes are mixed along the Δ direction, and in the LO mode the $SnCl_6^{2-}$ octahedron does not move while in the LA mode the Cs^+ cations remain stationary. Among the low-lying modes, only the longitudinal rotary and the longitudinal Q_6 modes remain pure.

Ignoring the intercell Cl–Cl bonding interactions in the short-range part of the potential affects the position and dispersion of the rotary mode Γ^{4+}. Thus if the second nearest-neighbor intercell Cl–Cl perpendicular force constant is ignored, the longitudinal rotary (LR) phonon branch is essentially flat along the Δ direction. Thus the model does not describe the softening of the rotary phonon mode seen in some A_2MX_6 lattices since the Γ^{4+} and X^{4+} phonon modes remain almost degenerate.

A linear interpolation tetrahedral method[25] was used to calculate the phonon density-of-states. The $^1/_{48}$th irreducible portion of thee Brillouin zone, defined by $0 \leq k_x \leq k_y \leq k_z \leq 2\pi/a$, $k_x + k_y + k_z \leq 3\pi/a$, was divided into a mesh of 89 points. The computer programs of Skriver[26] were used for the subdivision. The dynamical matrix $D_{ij}(\mathbf{k})$ was then diagonalized at each $\mathbf{k} = (k_x, k_y, k_z)$ mesh point. The irreducible wedge of the Brillouin zone was completely covered by connecting points. The contribution of each tetrahedron to the dos was evaluated by linearly interpolating the eigenvalues at the corners. The total phonon dos was found by summing such contributions over all tetrahedra for all 27 phonon branches. The calculated phonon dos $g(\omega)$ for Cs_2SnCl_6 is shown in Figure 5. To identify the origin of the peaks in the calculated phonon spectra, we note that the van Hove singularities in $g(\omega)$ correspond to high-symmetry regions of the Brillouin zone. Thus, using the calculated dispersion curves of Figure 4, we assign the peaks (Table III).

At energies greater than 100 cm^{-1}, all three experimental phonon frequency distribution functions (bfd at 12 K, tof at 80 and 298 K) show four peaks, which are easily assigned by comparison with the calculated phonon dos. Peak A can be assigned to the (unresolved) Γ^{1+} and Γ^{4-} internal stretching modes. Its asymmetry on the high-energy side arises from the longitudinal component of Γ^{4-}. Peak B is assigned to the Γ^{3+} internal stretching mode and its high-energy asymmetry to the X^{1+} (ν_2) zone-boundary phonon. Peak C is assigned to the unresolved Γ^{4-} and Γ^{5+} bending modes, with its high-energy asymmetry assigned to the longitudinal component of Γ^{4-}. Thus the intramolecular part of the phonon spectrum is dominated by zone-center modes, reflecting the limited dispersion of the internal modes. Peak D arises from the X^{5-} ($T\nu_6$) zone-boundary phonon mode and its low-energy asymmetry from the X^{3-} ($L\nu_6$) phonon mode. The ν_6 mode is inactive in both infrared and Raman spectroscopy. Its assignment is unambiguous since there are no external modes at energies larger than 100 cm^{-1}.

Table III. Composition of Calculated Phonon Dos Peaks in Cs_2SnCl_6

energy/cm^{-1}	assgnt	energy/cm^{-1}	assgnt
318	$L\nu_3$	107	$L\nu_6(X^{3-})$
313	$T\nu_3$	71	$TO(\Gamma^{4-})$
308	ν_1	64	$Rot(X^{5+})$, $Rot(L^{2+})$
247	ν_2 (X^{1+})	58	Rot (X^{4+})
244	ν_2	57	Rot (Γ)
182	$L\nu_4$	52	LCs^+ (Γ), $LA(L^{2-})$
172	$T\nu_4$	35	TA (X^{5-})
164	ν_5	25	TA (L^{3-})
109	$T\nu_6(X^{5-})$		

At energies lower than 100 cm^{-1}, peak E is assigned to the transverse branch of the optic mode (Γ^{4-}), consistent with its observation by infrared spectroscopy and its significant temperature dependence (70 cm^{-1} at 298 K, 80 cm^{-1} at 80 K), which arises from the contraction of the lattice. Peak F, in the region of the rotary mode Γ^{4+}, can be assigned to the L^{2+}(Rot) and X^{5+}(Rot) zone-boundary phonon modes. This assignment is supported by comparing the intensities of peaks E and F in both experimental and calculated phonon dos. Peak G is assigned to the Cs^+ motion lattice mode (Γ^{5+}) at the zone center. Contribution to this peak may also come from the L^{2-} zone-boundary branch of the longitudinal acoustic mode. Peaks I and K are not separated at ambient temperature, but they are clearly resolved at 80 K. Both arise from high-symmetry points corresponding to the acoustic mode and consistent with this assignment have a highly Q-dependent dispersion (scattering angles 13–110°). Peak I is assigned to the X^{5-} (TA) and peak K to the L^{3-} (TA) zone-boundary phonon modes.

Since only a limited amount of zone-center data has been used in the least-squares fitting and only a limited number of short-range interactions were taken into account, the calculated phonon dos for Cs_2SnCl_6 shows an encouraging agreement with the experimentally determined one, making it possible to assign all the observed phonon peaks. In particular we note the unambiguous identification of acoustic phonons in the low-energy part of the spectrum and of the silent ν_6 mode.

The calculated frequency of the X^{5-} ($T\nu_6$) mode is 109 cm^{-1}, while the observed values are 122 (tof at 298 K), 125 (tof at 80 K), and 124 cm^{-1} (bfd at 12 K). The observed ν_6 was then included into the least-squares fit to the OLW model (model II, Table II), increasing the parallel Cs–Cl force constant. In model II, Γ^{4+} is at 70 cm^{-1} while at the zone-boundary X^{5+} is 64 cm^{-1}, so the assignment of the phonon spectrum is unchanged.

Cs_2SbCl_6 Phonon Spectra. The unit cell of $Cs_4Sb^{III}Sb^{V}Cl_{12}$ is body-centered tetragonal[9] and involves a doubling of the pseudocubic antifluorite unit cell along the c axis. The primitive unit cell is shown in Figure 6 and the Brillouin zone in Figure 7. The number of $Cs_4Sb^{III}Sb^{V}Cl_{12}$ molecular units in the primitive unit cell is 2 and the number of atoms 36, thus resulting in 108 normal modes of vibration for each wave vector **k**. The Cartesian coordinates of the center of mass of each $SbCl_6$ unit are as follows: $Sb^{III}(1)$, (0, 0, 0); $Sb^{III}(2)$, (0, $^1/_2a$, $^1/_4c$); $Sb^{V}(3)$, ($^1/_2a$, $^1/_2a$, 0); $Sb^{V}(4)$, ($^1/_2a$, 0, $^1/_4c$). Further complications with the lattice dynamics analysis compared to that for Cs_2SnCl_6 are that the Sb–Cl separations are not equal around each $SbCl_6^{n-}$ unit and the positions of the Cs^+ cations are not determined by symmetry.

(24) Prassides, K. D.Phil. Thesis, Oxford University, 1984.
(25) Jepsen, O.; Andersen, O. K. *Solid State Commun.* **1971**, *9*, 1763. Lehmann, G.; Taut, M. *Phys. Status Solidi B* **1972**, *54*, 469. Rath, J.; Freeman, A. J. *Phys. Rev. B: Solid State* **1975**, *11*, 2109.
(26) Skriver, H. L. "The LMTO Method"; Springer Verlag: West Berlin, 1984; Vol. 41.
(27) Chodos, S. L.; Berg, R. W. *J. Chem. Phys.* **1979**, *70*, 4864.

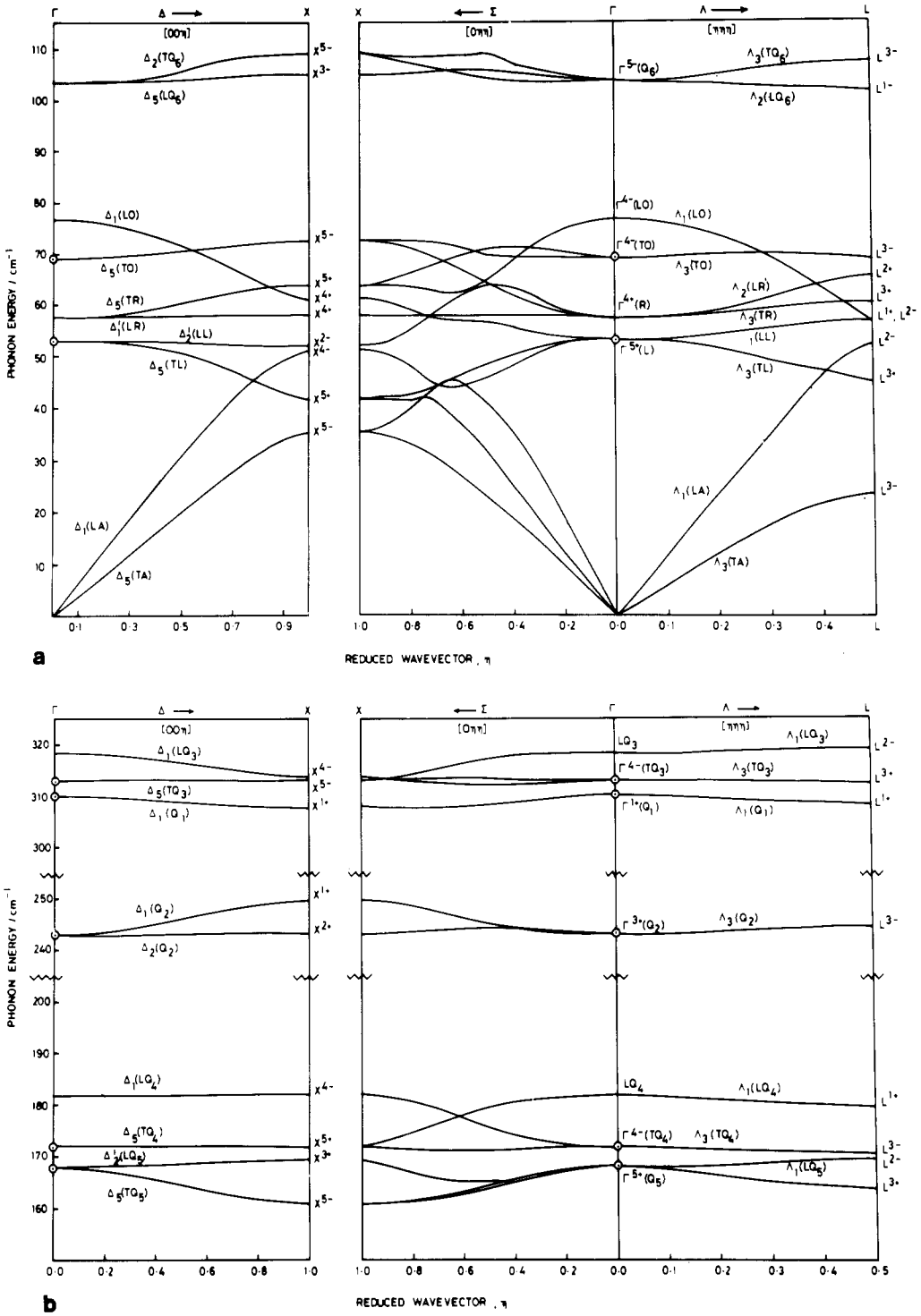

Figure 4. Calculated phonon dispersion for Cs_2SnCl_6 (model I): (a) energy < 120 cm^{-1}; (b) energy > 120 cm^{-1}.

Optical spectroscopy[4,6,7] provides frequencies of nine internal modes of the $SbCl_6^{3-}$ and $SbCl_6^-$ units and one external mode (the transverse optic mode). We assume the $SbCl_6^{n-}$ octahedra have Sb^V–Cl (or Sb^{III}–Cl) bond lengths equal to the average $Sb^{III,V}$–Cl[9] value and hence, in the short-range part of the dynamical matrix, restrict the interactions within each octahedron to the primitive unit cell. Then as in Cs_2SnCl_6, there are six symmetry-independent bonds, three for each valency state. These are bonding interactions between Sb(V) (or Sb(III)) and a Cl ion, Sb(3)–Cl(17) (or Sb(1)–Cl(5)), between nearest-neighbor Cl ions, Cl(17)–Cl(18) (or Cl(5)–Cl(6)) and between axially symmetric Cl ions, Cl(17)–Cl(19) (or Cl(5)–Cl(7)). If the Cs^+ ion lies in the tetrahedral hole in the lattice, one need consider only four symmetry-independent Cs–Cl bonds, namely Cs–Cl_{eq}^V, Cs–Cl_{ax}^V, Cs–Cl_{eq}^{III}, and Cs–Cl_{ax}^{III}. Further, there are two symmetry-independent near-neighbor Cs–Cs bonding interactions, because of the tetragonal distortion along the c axis, namely $c > 2a$. Thus, there are 12 independent pairs of atoms within each primitive unit cell.

Since there are 10 observed frequencies of the normal modes at the Γ point, interactions between the Cl atoms on neighboring octahedra are ignored. Within our model such coupling is provided only by the Cs–Cl force constants.

Three more independent parameters are included in the long-range part of the dynamical matrix, namely q_{Cl}, $q_{Sb(III)}$, and $q_{Sb(V)}$. Preservation of electrical neutrality determines the charge of the Cs cations, and we further assume that $q_{Cl(III)} \sim q_{Cl(V)}$ and that all the Cs ions have the same charge, though they are not symmetry equivalent.

The equilibrium conditions of Boyer and Hardy[21] again help to limit the number of independent parameters. The equilibrium

Table IV. Lattice Dynamics Parameters for $CsM^{III}_{0.5}Sb^{V}_{0.5}Cl_6$ (M = Sb, Bi, Tl)

	Atom Charges (e)					
M(III) 1.0	Sb(V) 1.4		Cl −0.4	Cs 0.6		
	force constant/N m^{-1}					
	parallel/$\Phi_\parallel$			perpendicular/$\Phi_\perp$		
	Sb	Bi	Tl	Sb	Bi	Tl
Cs–Cs	−0.2	−0.2	−0.2	0	0	0
Cs–Cl	6.0	6.0	6.0	0	0	0
$Cl^{III}(5)$–$Cl^{III}(7)$	16.6	21.7	7.7	0	0	0
$Cl^{V}(17)$–$Cl^{V}(19)$	17.2	16.4	14.6	0	0	0
$Cl^{III}(5)$–$Cl^{III}(6)$	11.1	7.0	10.5	−5.9	−6.4	−7.6
$Cl^{V}(17)$–$Cl^{V}(18)$	7.7	8.4	9.6	−7.7	−7.4	−6.8
M(1)–$Cl^{III}(5)$	55.9	60.7	83.5	14.9	15.4	22.4
Sb(3)–$Cl^{V}(17)$	162.2	160.7	164.5	29.9	30.4	24.7

	freq/cm^{-1}					
	Sb		Bi		Tl	
	obsd	calcd	obsd	calcd	obsd	calcd
Q_3^V	348	348	348	348	348	350
Q_1^V	324	327	326	327	329	331
Q_2^V	286	286	286	285	286	286
Q_1^{III}	257	257	255	255	264	263
Q_3^{III}	210	211	215	208	228	231
Q_2^{III}		(195)		(195)	192	194
Q_4^V	188	189	188	189	188	188
Q_5^V	175	162	174	162	174	161
Q_4^{III}	170	158		(141)	142	142
Q_5^{III}	117	137	120	118	133	132

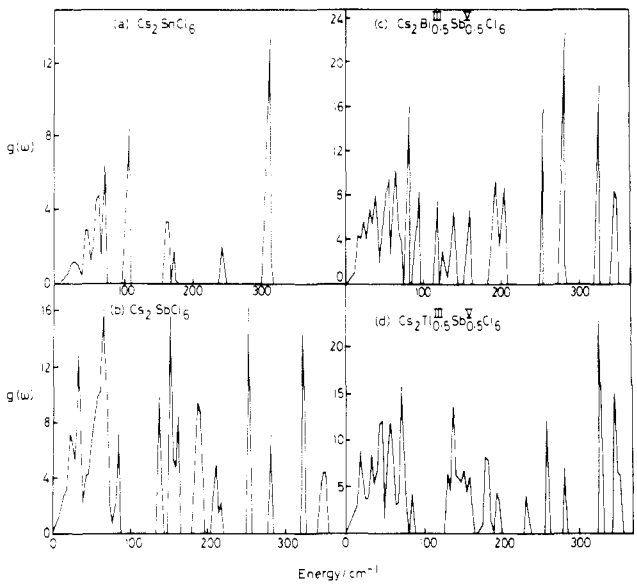

Figure 5. Calculated phonon dos $g(\omega)$ of (a) Cs_2SnCl_6, (b) Cs_2SbCl_6, (c) $Cs_2Sb_{0.5}Bi_{0.5}Cl_6$, and (d) $Cs_2Tl_{0.5}Sb_{0.5}Cl_6$.

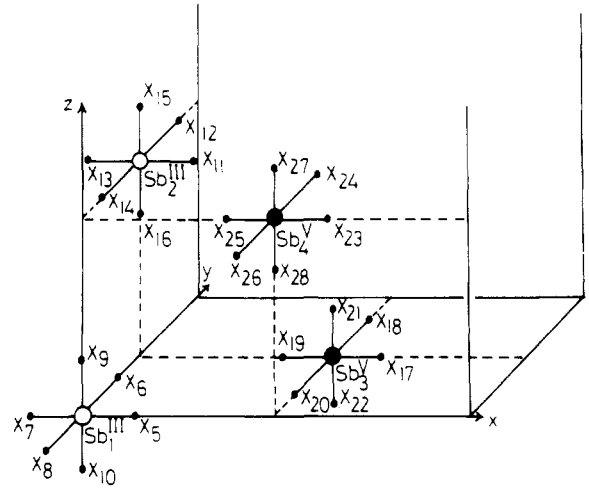

Figure 6. Portion of unit cell of body-centered-tetragonal A_2SbX_6, showing the numbering scheme used in the model.

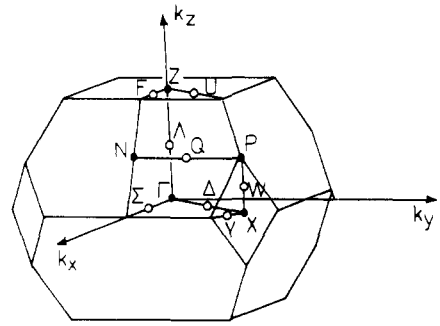

Figure 7. Body-centered-tetragonal Brillouin zone appropriate for Cs_2SbCl_6 ($c > a$).

condition that, for the Cl atoms, the forces must lie along the Sb^V–Cl or the Sb^{III}–Cl bond reduces the number of independent parameters by two while the second condition that the total macroscopic stress must be equal to zero provides two more constraints on the perpendicular force constants.

As with Cs_2SnCl_6, the perpendicular force constants of the bonds Cs–Cs, Cs–Cl, Cl(5)–Cl(7), and Cl(17)–Cl(19) are set equal to zero. Further, because the differences in bond distances are small, the parallel force constants of the two symmetry-independent near-neighbor Cs–Cs interactions are set equal. The same approximation is applied to the four symmetry-independent Cs–Cl bonds. Thus the total number of independent parameters is reduced to 15. Using the four equilibrium conditions as part of the data and fitting them to zero bring the total number of data points to 14. Thus, we diagonalize the dynamical matrix, D (eq 4), with $i, j = 1$–108.

Due to the complexity of the model it was not possible to fit all 15 parameters. The five parameters excluded from the refinement were assigned values obtained from the Cs_2SnCl_6 lattice dynamical model: $\Phi//(Cs–Cs) = -0.2$ N m^{-1}, $\Phi//(Cs–Cl) = 6.0$ N m^{-1}, $q_{Cs} = +0.6$, $q_{Cl} = -0.4$, $q_{Sb(V)} = +1.4$, $q_{Sb(III)} = +1.0$. In view of the considerable similarity of the low-energy part of the experimental phonon spectra of Cs_2SnCl_6 and Cs_2SbCl_6, such an approximation seems justifiable. A further complexity in the

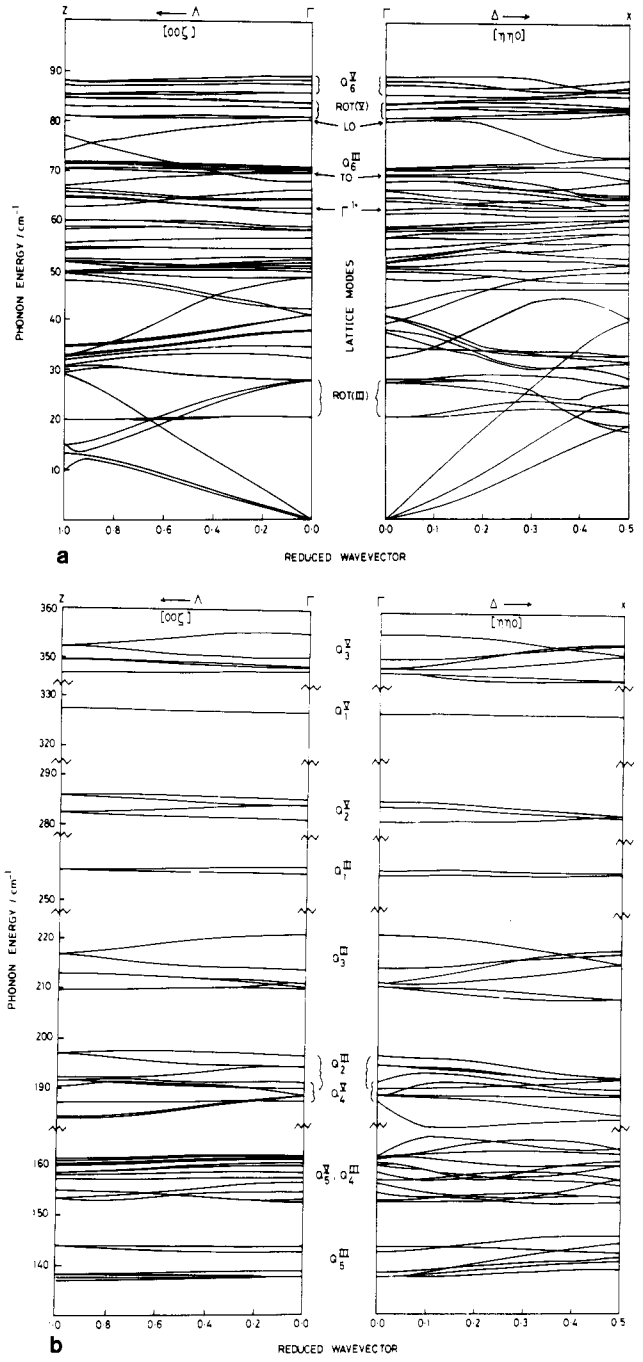

Figure 8. Calculated phonon dispersion in Cs_2SbCl_6: (a) below 120 cm^{-1}; (b) above 120 cm^{-1}.

model arises from the close proximity of the Q_5 mode of $Sb^{V}Cl_6^-$ (175 cm^{-1}) and the Q_4 mode of $Sb^{III}Cl_6^{3-}$ (170 cm^{-1}). Both decompose to a Γ^{5+} and a Γ^{5-} transverse branch in the tetragonal ordered structure, leading to extensive mixing of the phonon branches. The final least-squares-fitted parameters are listed in Table IV, with the observed and calculated values of the frequencies.

The final values of the force constants are substituted back into the dynamical matrix, and diagonalization along some high-symmetry lines of the Brillouin zone leads to the calculation of dispersion relations for Cs_2SbCl_6 (Figure 8). The eigenvectors[24] of the dynamical matrix indicate that for the high-energy branches of the internal modes there is very little mixing between the motions of the $SbCl_6^{3-}$ and $SbCl_6^-$ units at the Γ point, with the exception of Q_5^{V} and Q_4^{III} in which the two valency states are strongly coupled. The "silent" modes Q_6^{V} and Q_6^{III} (estimated frequencies of ca. 88 and 71 cm^{-1}) lie very close to external modes and strongly couple with the rotary mode involving rotation of the $SbCl_6^-$ units and the transverse optical mode, respectively. It

Table V. Composition of Calculated Phonon Dos in $Cs_2M^{III}_{0.5}Sb^{V}_{0.5}Cl_6$

	energy/cm^{-1}		
assignt	Sb	Bi	Tl
$L\nu_3^{V}$			356
$T\nu_3^{V}$	347	347	349
ν_1^{V}	328	328	331
ν_2^{V}	282	281	284
ν_1^{III}	256	255	262
$L\nu_3^{III}$	216		
$T\nu_3^{III}$	209	207	230
ν_4^{V}, ν_2^{III}	191	191	195
ν_5^{V}	165	161	161
$L\nu_4^{III}$			153
$T\nu_4^{III}$	153	139	139
$L\nu_5^{III}$		124	
$T\nu_5^{III}$	139	118	132
ν_6^{V}	86	94	85
Rot^{V}	82	80	
TO (Γ), Z^1	64	64	72
lat	58	55	56
lat	51		47
LA (Z)	33	36, 29	33
TA (X)	22	22, 18	19

is noteworthy that the rotary branches associated with rotation of the units of differing valency are well separated in frequency (ca. 82 and 25 cm^{-1}). Further, the frequency of the totally symmetric lattice mode, Γ^{1+} (62 cm^{-1}) is very close to that of the lattice mode ($\sim$60 cm^{-1}) that appears in the progression of ν_1^{V} ($n\nu_1^{V} + \nu_L$, n = 1, 2) in the resonance Raman spectrum of Cs_2SbCl_6.[4] If the eigenvectors along $\Lambda = \zeta(0, 0, 1)$ are followed, much more mode mixing is observed, with the transverse acoustic branches, for example, being strongly mixed with transverse rotary branches.

When the observed and calculated values of the frequencies are compared (Table IV) the largest discrepancies are found with the low-lying internal modes Q_5^{III}, Q_5^{V} and Q_4^{III}. Q_5^{III} lies at higher energy and the coupled Q_5^{V} and Q_4^{III} lie at lower energies, probably as a result of not including in the refinement the Cs–Cl and Cs–Cs force constants, which influence Q_5. Q_2^{III}, which has not been observed by optical spectroscopy, is predicted to lie at ca. 195 cm^{-1}, very close to Q_4^{V}.

To calculate the phonon dos of Cs_2SbCl_6, the irreducible portion of the Brillouin zone of Figure 7, defined by the relationships $0 \leq k_y \leq k_x \leq \pi/a$, $0 \leq k_z \leq 2\pi/c$, was divided into a mesh of 45 points. The calculated phonon dos $g(\omega)$ for Cs_2SbCl_6 is shown in Figure 5. Using the calculated dispersion curves (Figure 8), we can identify the origin of the peaks in the calculated phonon dos. The results of the assignments to phonons at the zone center or zone boundaries are presented in Table V.

This leads finally to the assignment of the peaks in the observed phonon frequency distribution functions (bfd at 12 K, tof at 80 and 298 K). The close similarity with the phonon spectra of Cs_2SnCl_6 is utilized in the identification of the peaks. Thus the intramolecular part of the phonon spectrum is dominated by zone-center modes, and all the peaks above 110 cm^{-1} can be assigned to internal modes at the Γ point. There is good agreement between frequencies observed by beryllium-filter and time-of-flight techniques (Table VI).

At energies lower than 110 cm^{-1}, identification of the peaks becomes more difficult because of the plethora of phonon branches. The peak at 99 cm^{-1} (298 K) or 101 cm^{-1} (80 K) in time-of-flight spectroscopy, which appears as a shoulder at 105 cm^{-1} in beryllium-filter spectroscopy, arises from the Q_6^{V} mode, which is inactive in both infrared and Raman spectroscopy. A very intense peak (54 and 57 cm^{-1} at 298 K, 60 and 62 cm^{-1} at 80 K) shows a small splitting and also a significant temperature dependence. By comparison with Cs_2SnCl_6, it is assigned to lattice modes, the temperature dependence arising from the contraction of the lattice. We assign the lower branch to the totally symmetric lattice mode at the zone boundary Z and the upper branch to the transverse optic mode at the zone center Γ. In a similar fashion the peak at 45 cm^{-1} is assigned to a lattice mode (Γ^{5+}). Furthermore, the

Table VI. Observed Frequencies in Phonon Spectra of Mixed-Valency and Mixed-Metal Salts (cm^{-1})

	Cs_2SbCl_6			$Cs_2Bi_{0.5}Sb_{0.5}Cl_6$	$Cs_2Tl_{0.5}Sb_{0.5}Cl_6$	$Rb_2Tl_{0.5}Sb_{0.5}Cl_6$	$Rb_{2.67}SbCl_6$
assgnt	bfd 12 K	tof 80 K	tof 295 K	tof 80 K	tof 295 K	tof 295 K	tof 80 K
$\nu_3{}^V$	348				345		
$\nu_1{}^V$			334		324		270
$\nu_2{}^{III}$	300		297		296	292	228
$\nu_1{}^{III}$	255		264		264	250	
$\nu_3{}^{III}$	228	234	230	234	230	230	183, 143
$\nu_4{}^V$, $\nu_2{}^{III}$		203	201	203, 220			116, 131
$\nu_5{}^V$, $\nu_4{}^{III}$	185, 168	184	177	182	175, 148	178, 148	93
$\nu_5{}^{III}$	124	127	122	125	125	122	
$\nu_6{}^V$	105	101	99	102	101	96	TO 74
$\nu_6{}^{III}$		82		78	86	82	Lat 56, 48
TO (Γ)		62	57	58	56	TO (Γ^{4-}) 68	A 41
Z		60	54				A 29
Lat (Γ^{5+})		47	44	46	46	LRb^+ (Γ^{5+}) 57	
LA(Z)		33	33	34	32	L^{3-} (TA) 41	
TA (X)		24		22		X^{5-} (TA) 37	

peak at 33 cm^{-1} arises from the longitudinal acoustic mode branch at the zone boundary Z. In the low-temperature phonon spectrum a weak shoulder at 22 cm^{-1} can be assigned to the transverse branch of the acoustic mode at the zone boundary X by comparison with the calculated phonon spectrum. The peak that appears at 80 K at 82 cm^{-1} is a good candidate for the $Q_6{}^{III}$ "internal" mode.

Ordered Mixed-Metal Salts. The lattice dynamical analysis of the $Cs_2Bi_{0.5}Sb_{0.5}Cl_6$ and $Cs_2Tl_{0.5}Sb_{0.5}Cl_6$ salts used the same model as for $Cs_2Sb^{III}_{0.5}Sb^{V}_{0.5}Cl_6$. The final values of the parameters at the end of the least-squares fit are tabulated in Table IV. The parallel and perpendicular force constants involving the $Sb^VCl_6^-$ units show only small variations, as expected. The force constants for $Bi^{III}Cl_6^{3-}$ and $Sb^{III}Cl_6^{3-}$ are very similar, as expected, since both Bi(III) and Sb(III) are s^2 "inert" pair ions, with the $Sb^{III}Cl_6^{3-}$ being slightly more strongly bonded. For $Tl^{III}Cl_6^{3-}$ the force constants $\Phi_\parallel$ and $\Phi_\perp$ of the M^{III}–Cl bond increase markedly, consistent with the s^0 electronic configuration of the Tl(III) ion.

The 45-point phonon dos for $Cs_2Bi_{0.5}Sb_{0.5}Cl_6$ and $Cs_2Tl_{0.5}Sb_{0.5}Cl_6$, shown in Figure 5, are very similar to the calculated phonon spectrum of Cs_2SbCl_6 and the results of the assignments are presented in Table V.

Again all the peaks of the experimental phonon frequency distribution functions ($Cs_2Bi_{0.5}Sb_{0.5}Cl_6$ at 80 K, $Cs_2Tl_{0.5}Sb_{0.5}Cl_6$ at 298 K) above 110 cm^{-1} can be assigned to intramolecular modes of the subunits at the Brillouin zone center. Identification of the peaks at energies lower than 110 cm^{-1} is made by comparison with Cs_2SbCl_6. Not surprisingly in view of the similarity of the incoherent cross sections of the elements (σ_{incoh} = 0.2, 0.25, and 0.1 × 10^{-28} m^2 for Sb, Bi, and Tl, respectively) and of the crystal structures and force field for the three salts $Cs_2M_{0.5}Sb_{0.5}Cl_6$ (M = Sb, Bi, Tl), their low-energy phonon spectra are almost identical.

$Rb_2Tl_{0.5}Sb_{0.5}Cl_6$ and $Rb_{2.67}SbCl_6$ Phonon Spectra. No lattice dynamical analysis was undertaken for $Rb_2Tl_{0.5}Sb_{0.5}Cl_6$ and $Rb_{2.67}SbCl_6$. $Rb_2Tl_{0.5}Sb_{0.5}Cl_6$ is disordered,[9] with a statistical distribution of $TlCl_6^{3-}$ and $SbCl_6^-$. The corresponding single-valent salts have different stoichiometries and crystal structures so one cannot average their force constants to model the lattice dynamics. Thus we identify the phonon peaks by comparison with $Cs_2Tl_{0.5}Sb_{0.5}Cl_6$. The crystal structure of $Rb_{2.67}SbCl_6$ is unknown so the spectrum will be discussed in terms of the zone-center optical information[3] and the Cs_2SbCl_6 phonon spectrum.

Besides the difference in mass between Cs and Rb, the major difference between $Cs_2Tl_{0.5}Sb_{0.5}Cl_6$ and $Rb_2Tl_{0.5}Sb_{0.5}Cl_6$ lies in the different incoherent cross sections of Cs and Rb. Thus Cs is a moderate neutron scatterer (σ_{incoh} = 3.2 × 10^{-28} m^2), while Rb does not scatter at all (σ_{incoh} = 0.0). Since the experimental phonon frequency distributions are weighted by the incoherent cross sections of the atoms involved, there are major differences in the intensities of phonon peaks that involve cation motions. Thus the phonon spectra of $Rb_2Tl_{0.5}Sb_{0.5}Cl_6$ and $Cs_2Tl_{0.5}Sb_{0.5}Cl_6$ are identical above 110 cm^{-1}, as expected, since the internal modes of $SbCl_6^-$ and $TlCl_6^{3-}$ are dominated by chlorine motions.

In contrast at low-energy transfer, the cation motions play a major role and the spectra differ markedly. In $Rb_2Tl_{0.5}Sb_{0.5}Cl_6$, the low-energy part of the spectrum is dominated by a single intense peak with a small spliiting (37 and 41 cm^{-1}), which corresponds to the acoustic mode involving the in-phase motion of all the elements in the primitive unit cell, including the chlorine atoms. On a face-centered-cubic unit cell we assign the two branches to the transverse acoustic phonon branches at the zone boundaries (L^{3-} and X^{5-}). The two intense peaks in $Cs_2Tl_{0.5}Sb_{0.5}Cl_6$ at 46 and 56 cm^{-1} were assigned to lattice modes; in $Rb_2Tl_{0.5}Sb_{0.5}Cl_6$, there are two weak peaks that appear as shoulders to the intense acoustic phonon peak at 57 and 68 cm^{-1}. It is consistent to assign these to the Rb^+ lattice mode and the transverse optic mode at Γ. The increased frequency results from the decrease in the mass of the cation. Two further weak peaks at 96 and 82 cm^{-1} are assigned to the $Q_6{}^V$ and $Q_6{}^{III}$ modes, and their diminished intensity indicates their strong coupling to lattice modes (Table VI).

Because of the reduction in crystal symmetry, the phonon spectrum of $Rb_{2.67}SbCl_6$ is poorly resolved. Furthermore, the negligible incoherent cross section of Rb results in low-intensity, almost unresolved, peaks in the low-energy part of the spectrum. Above 110 cm^{-1} the spectrum looks similar to the Cs_2SbCl_6 one at 80 K, but the asymmetries of the peaks indicate the larger dispersion of the phonon modes. The broad peak at 74 cm^{-1} is assigned to the transverse optic mode in agreement with the resonance Raman spectrum.[3] The peaks at 29 and 41 cm^{-1} probably arise from the components of the acoustic mode at the Brillouin zone boundaries. The results are summarized in Table VI.

Conclusions

Incoherent inelastic neutron scattering has provided information about the complete envelope of the phonon dos for Cs_2SbCl_6 and related mixed-metal salts up to and including the intramolecular Sb–Cl stretching modes in the region of 360 cm^{-1}, though the compounds are only moderate neutron scatterers and strong neutron absorbers. The lattice dynamics of the compounds modeled by the O'Leary and Wheeler rigid-ion model,[17] albeit with some simplifying approximations, lead to logical assignments of the observed peaks in the phonon spectra. Comparisons within the series $Cs_2M_{0.5}Sb_{0.5}Cl_6$ (M = Sb, Tl, Bi) or between $Rb_2Tl_{0.5}Sb_{0.5}Cl_6$ and $Cs_2Tl_{0.5}Sb_{0.5}Cl_6$ further improve the reliability of the results by demonstrating the consistency of the assignments.

It is also instructive to compare our force field model parameters of Cs_2SnCl_6 with those obtained by others. For example Chodos and Berg[27] calculated force constants for K_2SnCl_6 by taking into account Coulomb interactions and by using a modified Urey–Bradley force field to evaluate the short-range contributions to the dynamical matrix. They included only quadratic interactions for Sn–Cl, Cl–Cl, K–Cl, and K–K nearest-neighbor pairs. Further, they considered deformations of the Cl–Sn–Cl angles and assumed a fixed charge of +1.0 e for the potassium cation while fitting

the charge of the Cl ion. Further, the Cl ions were moved to the positions ($^1/_4$, 0, 0)a, i.e. to the center of the faces of the primitive cubic unit cell. Finally a quadratic interaction of the Cl–Cl intercell next-nearest-neighbor pairs was taken into account. Overall there is a very good agreement between their results and ours; e.g., they calculate the parallel Sn–Cl force constant to be 113.0 N m^{-1} (cf. 124.3 N m^{-1} for model I, 116.7 N m^{-1} for model II) and the Cl–Cl nearest-neighbor interaction, 22.4 N m^{-1} (cf. 17.9 N m^{-1} for model I, 20.1 N m^{-1} for model II). The differences partly arise from their neglect of the perpendicular Sn–Cl and the nonrefinement of the perpendicular Cl–Cl force constant that was fixed at −2.4 N m^{-1} (cf. −4.0 N m^{-1} for model I, −3.2 N m^{-1} for model II). The parallel K–Cl and K–K force constants were estimated to be 5.5 and −1.8 N m^{-1}, respectively, while our values for Cs–Cl and Cs–Cs are 6.1 (or 6.5 for model II) and −0.2 N m^{-1}, respectively. Further, the intercell Cl–Cl parallel force constant is estimated as only −0.4 N m^{-1}. Hence our results agree quite well except for the charge of Sn^{IV} which is estimated as 0.4 e (cf. 1.2 e for model I, 0.9 e for model II).

Overall, the structural and vibrational data now available reveal a remarkable similarity between the ground-state vibrational properties of mixed-valency Cs_2SbCl_6 and the mixed-metal related salts $Cs_2M_{0.5}Sb_{0.5}Cl_6$. The evolution of the structure with temperature[9] shows no dramatic changes, with only an approximately isotropic expansion effect. The parts of the phonon spectra arising from lattice modes are almost identical, while at higher energy, the spectra are a simple superposition of the individual properties of the single-valent ions with no measurable effect of mixed valency. This is consistent with the strongly localized nature (class II) of Cs_2SbCl_6. However, the excited-state properties are not a simple superposition of the properties of the constituent ions, because in Cs_2SbCl_6 and $Cs_2Bi_{0.5}Sb_{0.5}Cl_6$, there is an intervalence state Sb(IV)–Sb(IV) or Bi(IV)–Sb(IV) only ∼1.5 or ∼3 eV above the ground state.

Furthermore, we have accumulated enough information (a set of force constants and ionic charges) to be able to estimate the change both in elastic and Coulomb energy in going from the mixed-valency $Cs_2Sb^{III}_{0.5}Sb^{V}_{0.5}Cl_6$ to the single-valency compound $Cs_2Sb^{IV}Cl_6$. This allows an estimation of the one-center Coulomb repulsion energy U (for a quantitative discussion see ref 28).

The intervalence charge-transfer band in mixed-valency hexachloroantimonates(III,V) has been discussed in detail.[2,11] Enough experimental information exists to construct quantitatively the one-dimensional potential energy surface in the important vibrational coordinate q, the antisymmetric combination of the totally symmetric modes of the individual subunits. However, close examination of the temperature dependence of the intervalence band and its low-energy tail clearly demonstrates the inadequacy of a one-dimensional model and the necessity of coupling low-frequency lattice motions to the intervalence transition. Thus the shape function of each vibronic line (so far assumed to be a δ function) may be convoluted by the weighted dos of the lattice phonons, $g(\omega)$. In this way, the broadening of the absorption envelope and the lack of vibronic structure can be accounted for in a consistent way without recourse to arbitrary broadening of the vibronic lines, as in the PKS model[29] where each line is taken as a Gaussian with an artificial half-width of 2.4 ν_q. Ballhausen,[30] for example, uses such a convolution to account for the contributions of multiphonon processes to the shape of absorption spectra of impurities embedded in a matrix. The gross shape of the absorption spectrum is s determined by the internal vibrations of the guest, but the shape of the individual absorption lines is governed by the coupling to the lattice phonons.

Acknowledgment. We thank Dr. M. Bee for his help with the IINS experiments and the Institut Laue-Langevin for providing neutron beam time. Drs. M. Sutton and H. Skriver have given invaluable help by providing copies of their computer programs. K.P. is a Research Fellow of St. Anne's College and also thanks Christ Church, Oxford, for a Senior Scholarship.

Registry No. Cs_2SnCl_6, 17362-93-5; Cs_2SbCl_6, 17805-64-0.

(28) Prassides, K.; Day, P. *Inorg. Chem.* **1985**, *24*, 1109.
(29) Piepho, S. B.; Krausz, E. R.; Schatz, P. N. *J. Am. Chem. Soc.* **1979**, *101*, 2730.
(30) Ballhausen, C. J. "Molecular Electronic Structures of Transition Metal Complexes"; McGraw-Hill: New York, 1979.